

Active nematic liquid crystals under a quenched random field

Yutaka Kinoshita and Nariya Uchida*

Department of Physics, Tohoku University, Sendai 980-8578, Japan

(Dated: May 9, 2024)

Coupling between flow and orientation is a central issue in understanding the collective dynamics of active biofilaments and cells. Active stresses generated by motor activity destroy (quasi-)long-range orientational order and induce chaotic vortex flows. In cellular and subcellular environment, alignment is also hindered by heterogeneous filamentous structures in extracellular matrix and various organelles in a cell. Here we address the effects of a quenched random field on the flow patterns and orientational order in two-dimensional active nematic liquid crystals. We found that the director dynamics is frozen above a critical disorder strength. For sufficiently strong randomness, the orientational correlation function decays exponentially with the distance, reproducing the behavior of passive random-field nematics. In contrast, the flow velocity decreases only gradually as the randomness is increased, and develops a logarithmic spatial correlation for strong disorder. The threshold between the activity- and disorder-dominated regimes is specified and its dependence on the activity parameter is discussed.

Introduction. – Collective motion of cells and biofilaments are of vital importance to life at various stages, such as cell division, morphogenesis, cell migration and apoptosis. The dynamics is driven by molecular motors and facilitated by orientational ordering of active elements that have slender shapes. While apolar interaction induces nematic order, active stresses generated by motor activity destroy (quasi-)long-range orientational order and generate chaotic flows with many vortices, which are known as active turbulence [1–3]. The active nematic turbulence was demonstrated in a two-dimensional suspension of microtubules and kinesin-motor-complexes[4]. Topological defects are also found in colonies of cells [5–7] and multicellular organisms [8], and their biological functions have been revealed.

The flow patterns of active nematics can be controlled by friction with the substrate [9–14], external fields [15–17], and confinement [18–23]. The effects of uniform external field has been studied theoretically. A model of an active pump using a Frederiks twisted cell [15]. A three-dimensional simulation of active nematics under an electric field found a direct transition from the active turbulence to a uniformly aligned state [16], while a laning state intervenes in two dimensions [17]. Laning states are also obtained in numerical simulations with isotropic [12, 13] or anisotropic [14] friction, and explored experimentally [9]. Confinement also results in various director patterns such as the laning state and vortex lattice [19–23]. Recently, attentions have extended to couplings of active nematics with non-uniform fields, such as friction by micropatterned surfaces [24], curvature of epithelial tissues [25], spatially varying activity [26, 27] and composition [28].

On the other hand, the behavior of active nematics in a randomly heterogeneous environment is an open issue. Cells in tissues are in contact with extracellular matrix that contain fibrous material such as cellulose of collagen. Collagen fibers form anisotropic networks that guide migration of cells. [29]. Plant cellulose is also used as a scaffold for in vitro culture of neural stem cells [30]. Microtubules in cells are entangled with other components of cytoskeletal networks such as actins

and intermediate filaments, which hinder alignment. The cytoplasm also contains a number of proteins that cyclically change their shapes and generate random hydrodynamic forces. They not only enhance diffusion in the cell [31], but also may contribute to disorientation of active cytoskeletal filaments. To elucidate the effects of heterogeneous anisotropic environments on active nematic flows, we address the effects of quenched random fields in this paper. The effect of a quenched random field on nematic liquid crystals has been studied in a model of nematic elastomers [32]. The numerical study showed that the orientational correlation function decays exponentially as a function of the distance, and that the correlation length also decays exponentially with the disorder strength. Recently, the effects of a random field on dry and wet active nematics have been addressed in Refs. [33, 34]. In both cases, the quenched disorder slows the dynamics of topological defects. The orientational correlation follows a crossover from algebraic to exponential decay for a dry active nematics, while a slow coarsening behavior is observed for wet active nematics. In the present paper, we widely vary the disorder strength and focus on dynamical steady states after coarsening stops.

Model. – The orientational order of a two-dimensional nematic liquid crystal is described by the symmetric and traceless tensor $Q_{ij} = S \left(n_i n_j - \frac{1}{2} \delta_{ij} \right)$, where S is the scalar order parameter and $\mathbf{n} = (\cos \theta, \sin \theta)$ is the director. The dynamical equations of active nematics in the dimensionless form read [2]

$$(\partial_t + \mathbf{v} \cdot \nabla) \mathbf{v} = \frac{1}{Re} \nabla^2 \mathbf{v} - \nabla p + \nabla \cdot \boldsymbol{\sigma} \quad (1)$$

and

$$(\partial_t + \mathbf{v} \cdot \nabla) \mathbf{Q} = \lambda S \mathbf{u} + \mathbf{Q} \cdot \boldsymbol{\omega} - \boldsymbol{\omega} \cdot \mathbf{Q} + \gamma^{-1} \mathbf{H}. \quad (2)$$

Here, \mathbf{v} is the normalized flow velocity which satisfies the incompressibility condition $\nabla \cdot \mathbf{v} = 0$, p is the pressure and $\boldsymbol{\sigma}$ is the stress tensor. The flow properties are characterized by the Reynolds number Re , the flow alignment parameter λ , and the rotational viscosity γ , and $u_{ij} = (\partial_i v_j + \partial_j v_i)/2$ and $\omega_{ij} = (\partial_i v_j - \partial_j v_i)/2$ are the symmetric and antisymmetric parts of

* nariya.uchida@tohoku.ac.jp

velocity gradient tensor, respectively. Hereafter we call $\omega = \omega_{xy}$ the vorticity. We assume $0 < \lambda < 1$; a positive value of λ corresponds to elongated or rod-like elements and $|\lambda| < 1$ to the flow-tumbling regime where no stable director orientation exists in a uniform shear flow [35, 36]. The molecular field H_{ij} is the symmetric and traceless part of $-\delta F/\delta Q_{ij}$, and is obtained from the Landau-de Gennes free energy [35]

$$F = \int f d^2r, \quad (3)$$

$$f = \frac{A}{2} \text{Tr} \mathbf{Q}^2 + \frac{C}{4} (\text{Tr} \mathbf{Q}^2)^2 + \frac{K}{2} (\nabla \mathbf{Q})^2 - \frac{1}{2} \mathbf{E} \cdot \mathbf{Q} \cdot \mathbf{E}. \quad (4)$$

The first two terms of the free energy density control the magnitude of the scalar order parameter S . Note that the term proportional to $\text{Tr} \mathbf{Q}^3$ identically vanishes for the two-dimensional nematic order parameter. The third term is the Frank elastic energy under the one-constant approximation, and the fourth term describes the coupling to the quenched random field \mathbf{E} . The molecular field is obtained as

$$H_{xx} = - (2A + CS^2) Q_{xx} + 2K \nabla^2 Q_{xx} + \frac{1}{2} (E_x^2 - E_y^2). \quad (5)$$

$$H_{xy} = - (2A + CS^2) Q_{xy} + 2K \nabla^2 Q_{xy} + E_x E_y. \quad (6)$$

The stress tensor is the sum of the passive stress

$$\boldsymbol{\sigma}^e = -\lambda S \mathbf{H} + \mathbf{Q} \cdot \mathbf{H} - \mathbf{H} \cdot \mathbf{Q}, \quad (7)$$

and the active stress

$$\boldsymbol{\sigma}^a = -\alpha \mathbf{Q}. \quad (8)$$

We assume an extensile active stress and hence the activity parameter α is positive.

We model the quenched random field to be of the form

$$\mathbf{E} = E_0 \mathbf{e}(\mathbf{r}) \quad (9)$$

where $\mathbf{e}(\mathbf{r}) = (\cos \theta_e, \sin \theta_e)$ is a random unit vector with its angle θ_e being a uniformly random number in $[0, 2\pi]$. Therefore, it satisfies

$$\langle \mathbf{e}(\mathbf{r}) \mathbf{e}(\mathbf{r}') \rangle = \frac{1}{2} \mathbf{I} \xi_e^2 \delta(\mathbf{r} - \mathbf{r}'), \quad (10)$$

where ξ_e is the correlation length of the random field. The contributions of the the random field and Frank elasticity to the free energy are estimated as $E_0^2 S_0$ and KS_0^2/l_Q^2 , respectively, where S_0 is the typical magnitude of the scalar order parameter and l_Q is the correlation length of \mathbf{Q} . The orientational correlation length becomes smaller for a stronger random field, and its lower bound is given by $l_Q \sim \xi_e$. Therefore, we define the effective disorder strength as

$$D_K = \frac{E_0^2 \xi_e^2}{KS_0}. \quad (11)$$

On the other hand, the contributions to the molecular field by the random field and the active stress are estimated as E_0^2 and

α , respectively. Thus we are led to the other definition of the dimensionless disorder strength,

$$D_\alpha = \frac{E_0^2}{\alpha}. \quad (12)$$

Disorder-dominated regime. – In the disorder dominated regime with $D_K \gg 1$ and $D_\alpha \gg 1$, the director will align with the local director and get frozen. In this case, we have approximately $\mathbf{n}(\mathbf{r}) = \mathbf{e}(\mathbf{r})$, $\mathbf{H} = \mathbf{0}$ and $\boldsymbol{\sigma}^e = \mathbf{0}$ in the stationary state, and the Frank elastic term in the molecular field is negligible. Thus, from Eqs.(5),(6), the scalar order parameter satisfies

$$-S (2A + CS^2) + E_0^2 = 0, \quad (13)$$

the solution of which is identified with S_0 . The nematic order parameter is given by

$$\mathbf{Q}(\mathbf{r}, t) = S_0 \left[\mathbf{e}(\mathbf{r}) \mathbf{e}(\mathbf{r}) - \frac{1}{2} \mathbf{I} \right]. \quad (14)$$

Since the molecular field is balanced and vanishes in the steady state, the flow velocity is determined solely by the active stress. For $\text{Re} \ll 1$, the velocity field is obtained by dropping the terms on the left hand side of Eq.(1) as

$$0 = \frac{1}{\text{Re}} \nabla^2 \mathbf{v} - \nabla p + \nabla \cdot \boldsymbol{\sigma}^a. \quad (15)$$

Solving (15) under the incompressibility condition and with (8), we obtain the velocity field in the Fourier representation,

$$\mathbf{v}^k = -\alpha \text{Re} \frac{\mathbf{I} - \hat{\mathbf{k}}\hat{\mathbf{k}}}{k^2} \cdot (ik \cdot \mathbf{Q}^k), \quad (16)$$

which gives the velocity structure factor

$$\begin{aligned} \Sigma_v(\mathbf{k}) &= \langle |\mathbf{v}^k|^2 \rangle \\ &= \frac{(\alpha \text{Re})^2}{k^2} \left(\langle |\hat{\mathbf{k}} \cdot \mathbf{Q}^k|^2 \rangle - \langle |\hat{\mathbf{k}} \cdot \mathbf{Q}^k \cdot \hat{\mathbf{k}}|^2 \rangle \right). \end{aligned} \quad (17)$$

The correlation function of the nematic order parameter reads from Eqs.(10,14) as

$$\langle Q_{ij}(\mathbf{r}) Q_{lm}(\mathbf{r}') \rangle = \frac{1}{4} S_0^2 \xi_e^2 (\delta_{il} \delta_{jm} + \delta_{im} \delta_{jl}) \delta(\mathbf{r} - \mathbf{r}'), \quad (18)$$

and accordingly

$$\langle Q_{ij}^k Q_{lm}^{-k} \rangle = \frac{1}{4} S_0^2 \xi_e^2 (\delta_{il} \delta_{jm} + \delta_{im} \delta_{jl}). \quad (19)$$

Substituting this into Eq.(17), we obtain

$$\Sigma_v(\mathbf{k}) = \frac{(\alpha \text{Re} S_0 \xi_e)^2}{4k^2}. \quad (20)$$

The velocity correlation function in the real space is given by the inverse Fourier transform of $\Sigma_v(\mathbf{k})$ as

$$\langle \mathbf{v}(\mathbf{r}) \cdot \mathbf{v}(\mathbf{r}') \rangle = -\frac{(\alpha \text{Re} S_0 \xi_e)^2}{8\pi} \ln |\mathbf{r} - \mathbf{r}'|. \quad (21)$$

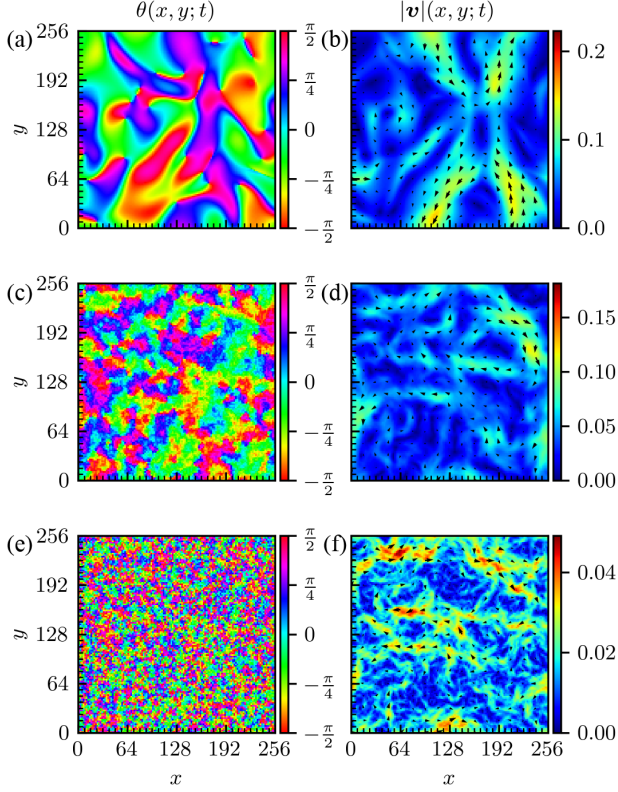


FIG. 1. Snapshots of the director angle $\theta(x, y)$ in the first column and velocity $\mathbf{v}(x, y)$ in the second column, for the field strength (a)(b) $E_0 = 0$, (c)(d) $E_0 = 0.4$, and (e)(f) $E_0 = 0.7$. The black arrows show the velocity field.

Numerical simulation. – We solved Eqs.(1,2) numerically on a square lattice with the fourth-order Runge-Kutta method. The incompressibility condition is handled by the simplified MAC method on a staggered lattice [37]. The main sublattice is used for the field variables \mathbf{Q} , p , $\boldsymbol{\sigma}$, \mathbf{u} , $\boldsymbol{\omega}$ and \mathbf{H} , and the other two sublattices are assigned to v_x and v_y . The calculation is performed on a $N_x \times N_y$ lattice with the grid size $\Delta x = \Delta y = 2$ and the step time increment $\Delta t = 0.01$. We assumed periodic boundary conditions and used Fast Fourier Transform to solve the Laplace equation for the pressure at each time step. For the numerical analysis, we used the parameter values

$$A = -0.16, C = 0.89, K = 1, \quad (22)$$

$$\lambda = 0.1, \text{Re} = 0.1, \gamma = 10, \alpha = 0.2. \quad (23)$$

The direction $\mathbf{e}(\mathbf{r})$ of the random field is randomly chosen at each grid point, which means $\xi_e = 2$. The field strength is varied in the range $0 \leq E_0 \leq 0.7$. The scalar order parameter in the passive ($\alpha = 0$) and stationary system is obtained from Eq.(13) as $S_0 \simeq 0.60$ for $E_0 = 0$ and $S_0 \simeq 0.96$ for $E_0 = 0.7$. The defect core radius is given by $\xi = \sqrt{K/|A|} \simeq 2.5$. The balance between the activity and Frank elasticity defines the lengthscale $l_\alpha = \sqrt{K/\alpha} \simeq 2.2$. The system size is fixed to $N_x = N_y = 128$ so that $L = N_x \Delta x = N_y \Delta y = 256$. For the initial conditions, we set the velocity to zero and assumed

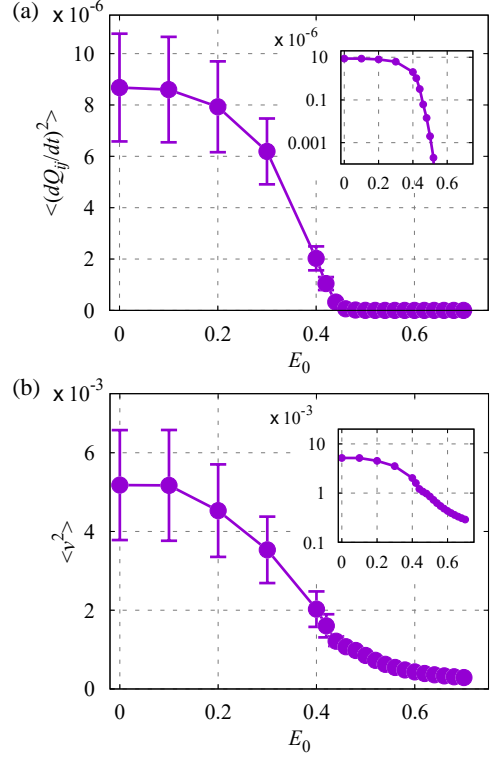


FIG. 2. Mean square of (a) the time-derivative of Q_{ij} and (b) flow velocity as a function of the field strength. Error bars show the standard deviation in the time course averaged over 10 samples. Insets: semi-log plots.

small random fluctuations around zero for $\mathbf{Q}(\mathbf{r}, 0)$, assuming a quench from the isotropic quiescent state. To be precise, the scalar order parameter and the director angle at each grid point are randomly chosen in the ranges $[0, 0.1]$ and $[0, 2\pi]$, respectively. We observed the total kinetic energy as a function of time to confirm that the system reached dynamical steady states, typically by $t = 10000$ for active turbulence states. We calculated the data over the time window $40000 < t \leq 80000$ with the time interval $t_0 = 100$, and took the ensemble average over 10 independent samples.

Spatial patterns and orientational freezing. – In Fig. 1, we show the snapshots of the director angle $\theta(\mathbf{r}, t)$ and the vorticity $\omega(\mathbf{r}, t)$ in the dynamical steady states for $\alpha = 0.2$. For $E_0 = 0$, active turbulence containing topological defects and vortices are reproduced [Fig.1(a)(b)]. For $E_0 = 0.4$, the director pattern becomes jaggy while maintaining the characteristic large-scale structure of nematic defects. The velocity field is smoother but wiggly streams appear [Fig.1(c)(d)]. For $E = 0.7$, the director orientation becomes completely random, and the flow pattern obtains fibrous structures of various size and magnitude [Fig.1(e)(f)].

The dynamics slows down as we increase the field strength. In Fig. 2, we show the mean square of the time-derivative of the order parameter \dot{Q}_{ij} and flow velocity. The director shows a marked slowdown above $E_0 = 0.2$, and the decay

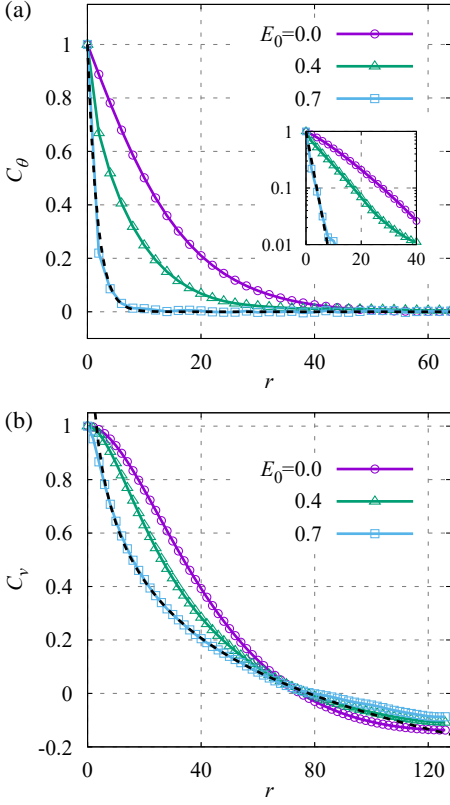


FIG. 3. (a) Director correlation function $C_\theta(r)$ (inset: semi-log plots). The dashed lines show the exponential function $\exp(-r/r_\theta)$ with $r_\theta = 1.7$. (b) Velocity Correlation function. The dashed line shows the logarithmic function $-A \ln(r/r_v)$ with $A = 0.31$ and $r_v = 78$.

becomes almost exponential above $E_0 = 0.44$, at which \dot{Q}_{ij}^2 is already below 4 percent of its value at $E_0 = 0$. The director dynamics completely freezes at $E_0 = 0.52$. On the other hand, the mean square velocity decreases only gradually as we increase the randomness. The decay above $E_0 = 0.44$ is roughly exponential but has a much smaller decay rate than that of the director. For $E_0 = 0.7$, the strongest field we studied, the mean square velocity still remains at about 6 percent of its value at $E_0 = 0$. Note that the effective disorder strengths are $D_K \simeq 0.97$ and $D_\alpha \simeq 0.96$ for $E_0 = 0.44$, which are both close to unity. Therefore, it would be reasonable to discriminate the medium and strong disorder regimes at this value of E_0 .

Correlation functions and correlation lengths. – In Fig. 3, we show the spatial correlation functions for the director angle and flow velocity, which are defined by

$$C_\theta(\mathbf{r}) = \frac{\langle \theta(\mathbf{r} + \mathbf{r}', t) \theta(\mathbf{r}', t) \rangle}{\langle \theta(\mathbf{r}', t)^2 \rangle} \quad (24)$$

and

$$C_v(\mathbf{r}) = \frac{\langle \mathbf{v}(\mathbf{r} + \mathbf{r}', t) \cdot \mathbf{v}(\mathbf{r}', t) \rangle}{\langle \mathbf{v}(\mathbf{r}', t)^2 \rangle}, \quad (25)$$

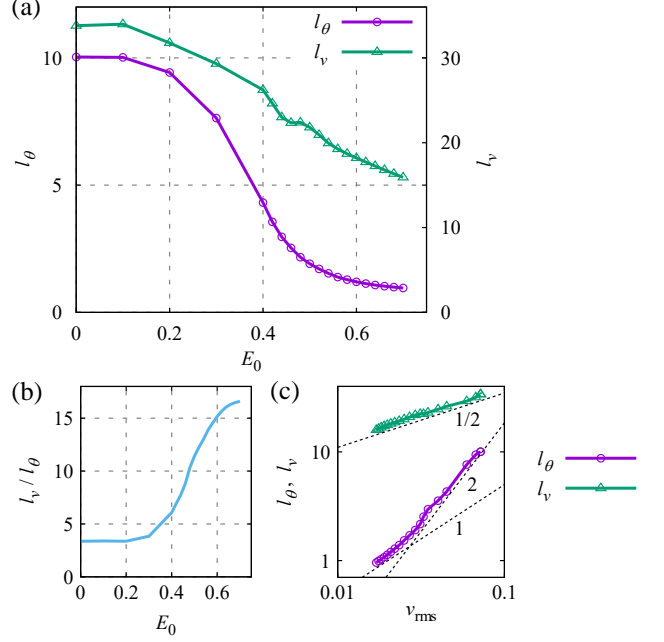


FIG. 4. (a) The director correlation length l_θ and velocity correlation length l_v as a functions of E_0 . (b) The ratio l_v/l_θ versus E_0 . (c) l_θ and l_v versus the mean flow velocity v_{rms} . The dashed lines show the power law $l \propto x^{1/2}$, x , x^2 .

respectively, where $\langle \dots \rangle$ indicates averages over \mathbf{r}' and t , and 10 independent samples. By symmetry, the correlation functions are functions of the distance only. We show their profiles along the x -axis in Fig. 3. The angular correlation function $C_\theta(r)$ is a monotonically decreasing function with a positive curvature [Fig. 3(a)]. For $E_0 = 0.7$, it is fitted by the exponential function $C_\theta(r) = \exp(-r/r_\theta)$ with $r_\theta = 1.7$. The semi-logarithmic plot in the inset of Fig. 3(a) shows that the exponential decay also holds for the medium disorder case $E_0 = 0.4$, up to $r \approx 30$.

The velocity correlation function decays more slowly than the angular one, and turns negative at $r \approx 0.3L$ for all the values of E_0 studied [Fig. 3(b)]. It is monotonically decreasing up to $r = 0.5L$, but should converge to zero for $r \rightarrow \infty$. The function has a negative curvature in a narrow range near $r = 0$, which becomes narrower for a larger field strength. For $E_0 = 0.7$, it is nicely fitted by the logarithmic function $C_v(r) = -A \ln(r/r_v)$ with $A = 0.31$ and $r_v = 78$, in the range $2 < r < r_v$.

We define the correlation lengths l_θ and l_v by $C_\theta(l_\theta) = 1/2$ and $C_v(l_v) = 1/2$, respectively. They are plotted in Fig. 4(a) as functions of the field strength. The angular correlation length shows a rapid decay between $E_0 = 0.2$ and 0.5 . The decay of the velocity correlation length is slower and roughly linear. The ratio l_v/l_θ plotted in Fig. 4(b) increases to 16 at $E_0 = 0.7$ from 3.4 at $E_0 = 0$. The correlation lengths are plotted versus the root mean square velocity $v_{rms} = \langle v^2 \rangle^{1/2}$ in Fig. 4(c). We find that $l_\theta \approx v_{rms}^{1/2}$ holds in the whole range, while l_v seems to scale as $l_v \approx v_{rms}^2$ in the weak disorder regime and crosses over to a slower decay with $l_v \approx v_{rms}$ in the strong disorder regime.

Discussion. – The exponential decay of the angular correlation function $C_\theta(r)$ in the strong and medium disorder regimes [Fig. 3(a)] is in agreement with the previous result on 2D random-field nematics [32]. This suggests that the director texture is determined by balance between the random field and Frank elasticity, and is little affected by the active flow. Earlier studies on the random-field XY model found correlation decay faster than exponential in two dimensions [38, 39]. The difference is attributed to the different symmetry of random anisotropy in nematics and the XY model [32]. Without the randomness, the angular correlation function decays faster than exponential as seen in Fig. 3(a). In this case, the correlation functions are characterized by the vortex size [40], and the velocity correlation function $C_v(r)$ has a negative curvature at short distances, as seen in Fig. 3(b) and in agreement with the analytical result [40]. As we increase the random field, the range with a negative curvature shrinks and the velocity correlation function is better approximated by the logarithmic function. This is in agreement with the analytical result for the strong disorder [Eq.(21)], and reflects the structure of the Green function of the Stokes equation in two dimensions. In three dimensions, the velocity correlation function should decay as $1/r$ in the strong disorder limit. Note also that the effective disorder strengths are $D_K \simeq 2.0$ and $D_\alpha \simeq 2.5$ for $E_0 = 0.7$, and are not large enough to ensure the constantness of the scalar order parameter. However, we confirmed that the correlation function for S decays to a constant at $r \simeq 2$, which underpins the agreement of $C_v(r)$ with the analytical result.

The dependences of the angular and velocity correlation lengths on the field strength are also in marked contrast. For weak disorder, both lengths are proportional to the vortex size and the ratio l_v/l_θ is small. For strong disorder, the velocity correlation decays only logarithmically even when the angular correlation length is zero, and thus l_v/l_θ diverges in the strong disorder limit. The slowing down of the increase of l_v/l_θ in the strong disorder regime [Fig. 4(b)] is explained by fact that the angular correlation length has a lower bound determined by the defect core size.

The apparent scaling of l_θ and l_v as functions of the mean flow velocity allows only partial interpretation. The dependence $l_v \approx v_{\text{rms}}$ in the strong disorder regime is understood by replacing ξ_e by ℓ_θ in the analytical result [Eq.(21)]. To be precise, using Eq. (17) with the characteristic wavenumber

$k \sim 1/l_\theta$ and its inverse Fourier transform, we obtain

$$v_{\text{rms}} \sim \alpha \text{Re} S_0 l_\theta. \quad (26)$$

The stronger dependence of l_v on v_{rms} in the weak disorder regime is a combined effect of activity, quenched disorder and Frank elasticity, for which analytical treatment is lacking. The previous studies [40, 41] suggested the scaling relations $l_\theta \propto \alpha^{-1/2}$ and $v_{\text{rms}} \propto \alpha^{1/2}$ for 2D active nematics with 2D orientational order parameter and without quenched disorder. It means that the active flow suppresses angular correlation and $l_\theta \propto v_{\text{rms}}^{-1}$. In contrast, the quenched disorder suppresses both angular correlation and active flow, and we found the positive correlation between the two.

Finally, we consider the competition between the active flow and random field. The flow-aligning effect on the nematic order parameter is represented by the term $\lambda S \mathbf{u}$ in Eq. (2), the magnitude of which is estimated as $\lambda S_0 v_{\text{rms}}/l_v$. The contribution of the random field in the term $\gamma^{-1} \mathbf{H}$ is estimated as $\gamma^{-1} E_0^2 S_0$. Averaging it over the area l_θ^2 of an orientationally correlated region, which contains $N \sim (l_\theta/\xi_e)^2$ sites, we get $\gamma^{-1} E_0^2 S_0 / \sqrt{N} \sim \gamma^{-1} E_0^2 S_0 \xi_e / l_\theta$. Thus the ratio between the flow-aligning and random-field terms is estimated as $\gamma \lambda v_{\text{rms}} l_\theta / (E_0^2 l_v \xi_e)$. In our simulation, this ratio becomes 0.25 for $E_0 = 0.2$, which confirms the observation that the active flow has a minor effect in the medium ($0.2 < E_0 < 0.44$) and strong ($E_0 > 0.44$) disorder regimes. It is also consistent the fact that the mean flow velocity and correlation lengths start to decrease around $E_0 = 0.2$. The dependence of the threshold on the activity parameter α is obtained by substituting $v_{\text{rms}} \propto \alpha$ and the scaling relation $l_\theta \sim l_v \sim l_\alpha = \sqrt{K/\alpha}$ (for $E_0 = 0$) into the above ratio, as $E_c \propto \alpha^{1/2}$. This dependence coincides with that of the stability threshold of the uniformly aligned state under an uniform external field [17], but has a different physical origin as we averaged the random field over an orientationally correlated region in the present work.

In summary, quenched disorder introduces unique twists into the physics of active nematics. For strong disorder, the director texture is frozen and determined by the balance between the randomness and Frank elasticity, while active flow with long-range correlation remains and facilitates material transport. We hope that the present work stimulates experimental studies on the flow properties of cellular and subcellular systems with orientational order.

Acknowledgements. – Yutaka KINOSHITA acknowledges support from GP-MS at Tohoku University.

[1] H. H. Wensink, J. Dunkel, S. Heidenreich, K. Drescher, R. E. Goldstein, H. Löwen, and J. M. Yeomans, Proc. Natl. Acad. Sci. U.S.A. **109**, 14308 (2012).

[2] A. Doostmohammadi, J. Ignés-Mullol, J. M. Yeomans, and F. Sagués, Nat. Commun. **9**, 1 (2018).

[3] R. Alert, J. Casademunt, and J.-F. Joanny, Ann. Rev. Condens. Matter Phys. **13**, 143 (2022).

[4] T. Sanchez, D. T. Chen, S. J. DeCamp, M. Heymann, and Z. Dogic, Nature **491**, 431 (2012).

[5] A. Doostmohammadi, S. P. Thampi, and J. M. Yeomans, Physical review letters **117**, 048102 (2016).

[6] T. B. Saw, A. Doostmohammadi, V. Nier, L. Kocgozlu, S. Thampi, Y. Toyama, P. Marcq, C. T. Lim, J. M. Yeomans, and B. Ladoux, Nature **544**, 212 (2017).

[7] K. Kawaguchi, R. Kageyama, and M. Sano, Nature **545**, 327 (2017).

[8] Y. Maroudas-Sacks, L. Garion, L. Shani-Zerbib, A. Livshits, E. Braun, and K. Keren, *Nature Physics* **17**, 251 (2021).

[9] P. Guillamat, J. Ignés-Mullol, and F. Sagués, *Proc. Natl. Acad. Sci. U.S.A.* **113**, 5498 (2016).

[10] P. Guillamat, J. Ignés-Mullol, S. Shankar, M. C. Marchetti, and F. Sagués, *Phys. Rev. E* **94**, 060602(R) (2016).

[11] P. Guillamat, J. Ignés-Mullol, and F. Sagués, *Nat. Commun.* **8**, 1 (2017).

[12] S. P. Thampi, R. Golestanian, and J. M. Yeomans, *Phys. Rev. E* **90**, 062307 (2014).

[13] P. Srivastava, P. Mishra, and M. C. Marchetti, *Soft Matter* **12**, 8214 (2016).

[14] K. Thijssen, L. Metselaar, J. M. Yeomans, and A. Doostmohammadi, *Soft Matter* **16**, 2065 (2020).

[15] R. Green, J. Toner, and V. Vitelli, *Phys. Rev. Fluids* **2**, 104201 (2017).

[16] Ž. Krajnik, Ž. Kos, and M. Ravnik, *Soft Matter* **16**, 9059 (2020).

[17] Y. Kinoshita and N. Uchida, *Physical Review E* **108**, 014605 (2023).

[18] L. Giomi, L. Mahadevan, B. Chakraborty, and M. Hagan, *Nonlinearity* **25**, 2245 (2012).

[19] A. Doostmohammadi, T. N. Shendruk, K. Thijssen, and J. M. Yeomans, *Nat. Commun.* **8**, 1 (2017).

[20] T. N. Shendruk, A. Doostmohammadi, K. Thijssen, and J. M. Yeomans, *Soft Matter* **13**, 3853 (2017).

[21] M. M. Norton, A. Baskaran, A. Opathalage, B. Langeslay, S. Fraden, A. Baskaran, and M. F. Hagan, *Phys. Rev. E* **97**, 012702 (2018).

[22] R. C. Coelho, N. A. Araújo, and M. M. T. da Gama, *Soft Matter* **15**, 6819 (2019).

[23] C. Rorai, F. Toschi, and I. Pagonabarraga, *Phys. Rev. Fluids* **6**, 113302 (2021).

[24] K. Thijssen, D. A. Khaladj, S. A. Aghvami, M. A. Gharbi, S. Fraden, J. M. Yeomans, L. S. Hirst, and T. N. Shendruk, *Proceedings of the National Academy of Sciences* **118**, e2106038118 (2021).

[25] F. Vafa and L. Mahadevan, *Physical Review Letters* **129**, 098102 (2022).

[26] J. Rønning, M. C. Marchetti, and L. Angheluta, *Royal Society Open Science* **10**, 221229 (2023).

[27] A. Partovifard, J. Grawitter, and H. Stark, *Soft Matter* **20**, 1800 (2024).

[28] R. Assante, D. Corbett, D. Marenduzzo, and A. Morozov, *Soft Matter* **19**, 189 (2023).

[29] G. Thrivikraman, A. Jagie Ilo, V. K. Lai, S. L. Johnson, M. Keating, A. Nelson, B. Schultz, C. M. Wang, A. J. Levine, E. L. Botvinick, and R. T. Tranquillo, *Proceedings of the National Academy of Sciences* **118**, e2024942118 (2021).

[30] L. J. Couvrette, K. L. Walker, T. V. Bui, and A. E. Pelling, *Bioengineering* **10**, 1309 (2023).

[31] A. S. Mikhailov and R. Kapral, *Proceedings of the National Academy of Sciences* **112**, E3639 (2015).

[32] Y.-K. Yu, P. Taylor, and E. Terentjev, *Physical review letters* **81**, 128 (1998).

[33] S. Kumar and S. Mishra, *Physical Review E* **102**, 052609 (2020).

[34] S. Kumar and S. Mishra, *Physical Review E* **106**, 044603 (2022).

[35] P.-G. De Gennes and J. Prost, *The Physics of Liquid Crystals* (Oxford University Press, 1993).

[36] S. Edwards and J. Yeomans, *EPL* **85**, 18008 (2009).

[37] A. A. Amsden and F. H. Harlow, *J. Comput. Phys.* **6**, 322 (1970).

[38] B. Diieny and B. Barbara, *Physical Review B* **41**, 11549 (1990).

[39] M. J. Gingras and D. A. Huse, *Physical Review B* **53**, 15193 (1996).

[40] L. Giomi, *Phys. Rev. X* **5**, 031003 (2015).

[41] E. J. Hemingway, P. Mishra, M. C. Marchetti, and S. M. Fielding, *Soft Matter* **12**, 7943 (2016).